NGTS-4b: A sub-Neptune Transiting in the Desert

Richard G. West,[1,2]* Edward Gillen,[3,†] Daniel Bayliss,[1,2] Matthew R. Burleigh,[5] Laetitia Delrez,[3] Maximilian N. Günther,[3] Simon T. Hodgkin,[7] James A. G. Jackman,[1,2] James S. Jenkins,[8,9] George King,[1,2] James McCormac,[1,2] Louise D. Nielsen,[4] Liam Raynard,[5] Alexis M. S. Smith,[6] Maritza Soto,[8] Oliver Turner,[4] Peter J. Wheatley,[1,2] Yaseen Almleaky,[15,16] David J. Armstrong,[1,2] Claudia Belardi,[5] François Bouchy,[4] Joshua T. Briegal,[3] Artem Burdanov,[14] Juan Cabrera,[6] Sarah L. Casewell,[5] Alexander Chaushev,[5,1,2] Bruno Chazelas,[4] Paul Chote,[1,2] Benjamin F. Cooke,[1,2] Szilard Csizmadia,[6] Elsa Ducrot,[14] Philipp Eigmüller,[6,10] Anders Erikson,[6] Emma Foxell,[1,2] Boris T. Gänsicke,[1,2] Michaël Gillon,[14] Michael R. Goad,[5] Emmanuël Jehin,[14] Gregory Lambert,[3] Emma S. Longstaff,[5] Tom Louden,[1,2] Maximiliano Moyano,[13] Catriona Murray,[3] Don Pollacco,[1,2] Didier Queloz,[3] Heike Rauer,[6,10,11] Sandrine Sohy,[14] Samantha J. Thompson,[3] Stéphane Udry,[4] Simon. R. Walker,[1,2] Christopher A. Watson[12]

[1] *Centre for Exoplanets and Habitability, University of Warwick, Gibbet Hill Road, Coventry CV4 7AL, UK*
[2] *Dept. of Physics, University of Warwick, Gibbet Hill Road, Coventry CV4 7AL, UK*
[3] *Astrophysics Group, Cavendish Laboratory, J.J. Thomson Avenue, Cambridge CB3 0HE, UK*
[4] *Observatoire de Genève, Université de Genève, 51 Ch. des Maillettes, 1290 Sauverny, Switzerland*
[5] *Department of Physics and Astronomy, Leicester Institute of Space and Earth Observation, University of Leicester, LE1 7RH, UK*
[6] *Institute of Planetary Research, German Aerospace Center, Rutherfordstrasse 2, 12489 Berlin, Germany*
[7] *Institute of Astronomy, Cambridge University, Madingley Road, Cambridge CB3 0HA, UK*
[8] *Departamento de Astronomia, Universidad de Chile, Casilla 36-D, Santiago, Chile*
[9] *Centro de Astrofísica y Tecnologías Afines (CATA), Casilla 36-D, Santiago, Chile.*
[10] *Center for Astronomy and Astrophysics, TU Berlin, Hardenbergstr. 36, D-10623 Berlin, Germany*
[11] *Institute of Geological Sciences, FU Berlin, Malteserstr. 74-100, D-12249 Berlin, Germany*
[12] *Astrophysics Research Centre, School of Mathematics and Physics, Queen's University Belfast, BT7 1NN Belfast, UK*
[13] *Instituto de Astronomía, Universidad Católica del Norte, Angamos 06010, 1270709, Antofagasta, Chile*
[14] *Space sciences, Technologies and Astrophysics Research (STAR) Institute, Université de Liège, 4000 Liège, Belgium*
[15] *Space and Astronomy Department, Faculty of Science, King Abdulaziz University, 21589 Jeddah, Saudi Arabia*
[16] *King Abdullah Centre for Crescent Observations and Astronomy, Makkah Clock, Mecca 24231, Saudi Arabia*
[†] *Winton Fellow*

ABSTRACT

We report the discovery of NGTS-4b, a sub-Neptune-sized planet transiting a 13th magnitude K-dwarf in a 1.34 d orbit. NGTS-4b has a mass $M = 20.6 \pm 3.0\,M_\oplus$ and radius $R = 3.18 \pm 0.26\,R_\oplus$, which places it well within the so-called "Neptunian Desert". The mean density of the planet ($3.45 \pm 0.95\,\mathrm{g\,cm^{-3}}$) is consistent with a composition of 100 % H_2O or a rocky core with a volatile envelope. NGTS-4b is likely to suffer significant mass loss due to relatively strong EUV/X-ray irradiation. Its survival in the Neptunian desert may be due to an unusually high core mass, or it may have avoided the most intense X-ray irradiation by migrating after the initial activity of its host star had subsided. With a transit depth of $0.13 \pm 0.02\%$, NGTS-4b represents the shallowest transiting system ever discovered from the ground, and is the smallest planet discovered in a wide-field ground-based photometric survey.

Key words: techniques: photometric, stars: individual: NGTS-4, planetary systems, planets and satellites: detection

arXiv:1809.00678v1 [astro-ph.EP] 3 Sep 2018

1 INTRODUCTION

Exoplanet population statistics from the Kepler mission reveals a scarcity of short period Neptune-sized planets (Szabó & Kiss 2011; Mazeh et al. 2016; Fulton & Petigura 2018). This so-called "Neptunian Desert" is broadly defined as the lack of exoplanets with masses around $0.1 \, M_J$ and periods less than 2–4 days (Szabó & Kiss 2011). As Neptune-sized planets should be easier to find in short period orbits, and many Neptunes have been discovered with longer orbits from surveys such as *CoRoT* and *Kepler*, this does not appear to be an observational bias. Ground-based surveys, which have uncovered the bulk of known hot Jupiters, have not uncovered these short-period Neptunes. However this may be due to the fact that such exoplanets produce transits too shallow for most ground-based surveys to detect.

The physical mechanisms that result in the observed Neptunian Desert are currently unknown, but have been suggested to be due to a different formation mechanism for short period super-Earth, and Jovian exoplanets, similar to the reasons for the brown dwarf desert (e.g. Grether & Lineweaver 2006). Alternatively, the dearth may be due to a mechanism stopping planetary migration. This may be a sudden loss of density within the accretion disk, or mass removed from the exoplanet via Roche lobe overflow (Kurokawa & Nakamoto 2014) or stellar X-ray/EUV insolation (Lopez & Fortney 2014) and evaporation of the atmosphere (Lecavelier Des Etangs 2007).

Owen & Lai (2018) investigated causes of the high mass/large radius and low mass/small radius boundaries of the desert. They showed that while X-ray/EUV photoevaporation of sub-Neptunes can explain the low mass/small radius boundary, the high mass/large radius boundary better corresponds to the tidal disruption barrier for gas giants undergoing high eccentricity migration. Their findings were consistent with the observed triangular shape of the desert, since photoevaporation is more prolific at shorter orbital periods, likewise more massive gas giants can tidally circularise closer to their stellar hosts.

Due to their shallow transits, Neptune-sized planets ($\approx 4 \, R_\oplus$) have largely eluded wide-field ground-based transit surveys such as WASP (Pollacco et al. 2006), HATNet (Bakos et al. 2004), HATSouth (Bakos et al. 2013), and KELT (Pepper et al. 2007, 2012). The notable exception is HAT-P-11b (Bakos et al. 2010), which has a radius of just $4.71 \pm 0.07 \, R_\oplus$. One other system worthy of note is the multi-planet system TRAPPIST-1 (Gillon et al. 2016), of which three of the Earth-sized planets were discovered from ground, however they orbit a late M-dwarf and their transit depths are in the range 0.6–0.8% (5–6 times larger than the depth of NGTS-4b), and surveys such as TRAPPIST and MEarth (Nutzman & Charbonneau 2008; Irwin et al. 2009) have specifically targeted M-dwarfs in order to maximise the detectability of small planets.

We present the discovery of a new sub-Neptune-sized ($R = 3.18 \pm 0.26 \, R_\oplus$) planet transiting a K-dwarf ($m_v = 13.1$ mag) in a $P = 1.33734$ d orbit from the Next Generation Transit Survey (NGTS) survey. In Sect. 2 we describe the NGTS discovery data. In Sect. 3 we describe our campaign of photometric follow-up on 1 m-class telescopes. In Sect. 4 we detail our spectroscopic follow-up including the mass determination via radial velocity monitoring. In Sect. 5
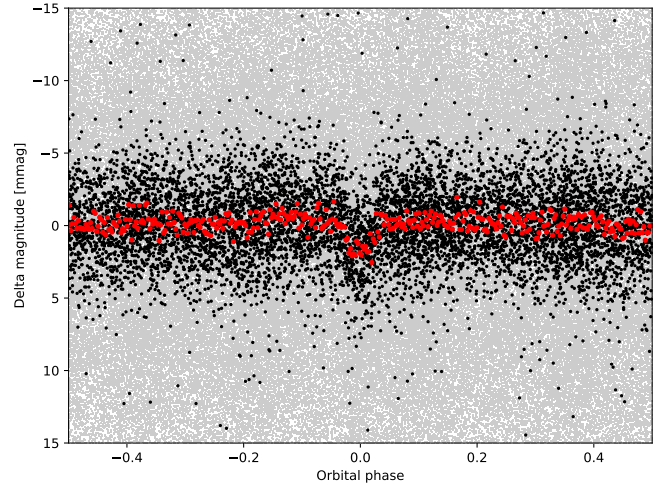

Figure 1. The NGTS discovery light curve of NGTS-4b. The data are shown phase-folded on the orbital period 1.33734 d. The grey points show the unbinned 10 s cadence data, the black dots are these data binned in linear time to a cadence of 5 min then phase-folded, and the red points are the unbinned data phase-folded then binned in phase to an equivalent cadence of 5 min.

we discuss our analysis of the stellar parameters and describe the global modelling process. In Sect. 6 we discuss the discovery in context with other planets in this mass/radius/period regime. Finally we finish with our conclusions in Sect. 7.

2 DISCOVERY PHOTOMETRY FROM NGTS

NGTS-4 was observed using a single NGTS camera over a 272 night baseline between 2016 August 06 and 2017 May 05. The survey has operated at ESO's Paranal observatory since early 2016 and consists of an array of twelve roboticized 20 cm telescopes. The facility is optimised for detecting small planets around K and early M stars (Wheatley et al. 2018; McCormac et al. 2017; Wheatley et al. 2013; Chazelas et al. 2012).

A total of 190 696 images were obtained, each with an exposure time of 10 s. The data were taken using the custom NGTS filter (550–927 nm) and the telescope was auto-guided using an improved version of the DONUTS auto-guiding algorithm (McCormac et al. 2013). The RMS of the field tracking errors was 0.051 pixels (0.26″) over the 272 night baseline. The data were reduced and aperture photometry was extracted using the CASUTools[1] photometry package. A total of 185 840 valid data-points were extracted from the raw images. The data were then de-trended for nightly trends, such as atmospheric extinction, using our implementation of the SysRem algorithm (Tamuz et al. 2005; Collier Cameron et al. 2006). We refer the reader to Wheatley et al. (2018) for more details on the NGTS facility and the data acquisition and reduction processes.

The complete dataset was searched for transit-like signals using ORION, an optimized implementation of the box-

---

[1] http://casu.ast.cam.ac.uk/surveys-projects/software-release

Table 1. Summary of photometry of NGTS-4. This table contains all the photometry of NGTS-4 from NGTS, Eulercam, LCO 1m, and SHOCa. A portion is shown here for guidance. The full table is available in a machine-readable format from the online journal.

Time (HJD-2450000)	Relative flux	Flux error	Filter	Instrument
7287.76965278	1.00973	0.01865	NGTS	NGTS
7287.76979167	1.01170	0.01861	NGTS	NGTS
7287.76994213	0.99010	0.01855	NGTS	NGTS
7287.77008102	1.00987	0.01860	NGTS	NGTS
7287.77023148	0.99255	0.01862	NGTS	NGTS
7287.77037037	0.99335	0.01858	NGTS	NGTS
7287.77052083	0.99226	0.01856	NGTS	NGTS
7287.77068287	0.99369	0.01859	NGTS	NGTS
7287.77082176	0.98936	0.01857	NGTS	NGTS
7287.77097222	1.02166	0.01867	NGTS	NGTS
...	...	...	...	...

fitting least-squares (BLS) algorithm (Kovács et al. 2002; Collier Cameron et al. 2006), and a ~0.2 % signal was detected at a period of 1.33734 d. The NGTS photometry, phase-folded to this period, is shown in Figure 1. A total of 28 transits are covered fully or partially by the NGTS dataset.

We find no evidence for a secondary eclipse or out-of-transit variation, both of which would indicate an eclipsing binary system. We used the centroid vetting procedure detailed in Günther et al. (2017) to check for contamination from background objects, and verify that the transit seen was not a false positive. This test is able to detect shifts in the photometric centre-of-flux during transit events at the sub-milli-pixel level. It can identify blended eclipsing binaries at separations below 1″, well below the size of individual NGTS pixels (5″). We find no signs of a centroiding variation during the transit events of NGTS-4.

Based on the NGTS detection and the above vetting tests, NGTS-4 was followed-up with further photometry and spectroscopy to confirm the planetary nature of the system and measure the planetary parameters. A sample of the full discovery photometry and follow-up data is given in Table 1, the full data are available in machine-readable format from the online journal.

3 PHOTOMETRIC FOLLOW-UP

Confirming such a shallow transit signal from the ground is challenging, even given some of the best 1 m-class telescopes available for precision time-series photometry. We therefore undertook a campaign of photometric follow-up using four different facilities as set out in this section. A summary of the photometric follow-up observations is given in Table 2, and the full data are available in machine-readable format in the online journal. The de-trended data are plotted in Figure 4 (see Sect. 5.2 for a description of the de-trending that has been applied to the data in these plots).

3.1 SHOC photometry

Our first follow-up photometry of NGTS-4 was carried out at the South African Astronomical Observatory (SAAO) on

2017 November 27, with the 1.0 m telescope and one of the three frame-transfer CCD Sutherland High-speed Optical Cameras (Coppejans et al. 2013, SHOC), specifically SHOC'n'awe. The SHOC cameras on the 1 m telescope have a pixel scale of 0.167″/pixel, which is unnecessarily fine for our observations, hence we binned the camera 4×4 pixels in the X and Y directions. All observations were obtained in focus, using a *V* filter and an exposure time of 30 s. The field of view of the SHOC instruments on the 1 m is 2.85′×2.85′, which allowed for one comparison star of similar brightness to the target to be simultaneously observed.

The data were bias and flat-field corrected via the standard procedure using the CCDPROC package (Craig et al. 2015) in python. Aperture photometry was extracted for NGTS-4 and the comparison star using the SEP package (Barbary 2016; Bertin & Arnouts 1996) and the sky background was measured and subtracted using the SEP background map. We also performed aperture photometry using the Starlink package AUTOPHOTOM. We used a 4 pixel radius aperture that maximised the signal/noise, and the background was measured in an annulus surrounding this aperture. The comparison star was then used to perform differential photometry on the target. Both photometry methods successfully detected a complete transit of NGTS-4b despite the observations being partially effected by thin cirrus during the transit.

NGTS-4 was observed again at SAAO with the 1 m telescope and the SHOC'n'awe instrument at the end of astronomical twilight on 2018 April 22. On this occasion sky conditions were excellent, with sub-arcsecond seeing throughout and a minimum of ≈ 0.6″ recorded. On this occasion the observations were made using an *I* filter. Initially, an exposure time of 5 s was used, but after the first 30 minutes this was reduced to 2 s as the target's flux was uncomfortably close to the non-linear regime of the CCD. These data were also reduced and analysed as described above, and the transit egress was clearly detected (Figure 4).

3.2 LCO 1 m

We monitored transit events of NGTS-4b using the Las Cumbres Observatory (LCO) 1 m global telescope network (Brown et al. 2013). All observations were taken using the Sinistro cameras, which give an a 26.5′ × 26.5′ field of view with a plate-scale of 0.389″/pixel. Exposure times were set to 180 s, with a defocus of 2 mm in order to ensure we did not saturate NGTS-4 and light was spread over a larger number of detector pixels. We used the *i*-band filter and the standard 1 × 1 binning readout mode. In total six events were monitored with the LCO 1 m telescopes from the sites in Chile and Australia. A full list of these events along with details of each observation are set out in Table 2.

Raw images were reduced to calibrated frames using the standard LCO "Banzai" pipeline. Aperture photometry was extracted for NGTS-4 and the 7 comparison stars using the SEP package (Barbary 2016; Bertin & Arnouts 1996) and the sky background was measured and subtracted using the SEP background map. The resulting light-curve shows the signature of a full transit (Figure 4).

3.3 Speculoos

We monitored a transit event using the SPECULOOS-South facility (Burdanov et al. 2017; Delrez et al. 2018) at Paranal Observatory in Chile on the night of 2018 April 15, taking advantage of the telescope commissioning period. SPECULOOS-South consists of four robotic 1-meter Ritchey-Chretien telescopes, and we were able to utilize two of these (Europa and Callisto) to observe the transit event. Given the shallowness of the targeted transit, we opted to maximise the flux from the early K host star and chose an I+z filter for both telescopes. SPECULOOS-South is equipped with a deep-depletion $2k \times 2k$ CCD camera with a field-of-view of $12' \times 12'$ ($0.35''$/pixel).

The images were calibrated using standard procedures (bias, dark, and flat-field correction) and photometry was extracted using the IRAF/DAOPHOT aperture photometry software (Stetson 1987), as described by Gillon et al. (2013). For each observation, a careful selection of both the photometric aperture size and stable comparison stars was performed manually to obtain the most accurate differential light curve of NGTS-4. The signature of a full transit is evident in the light-curves from both telescopes (Figure 4).

3.4 Eulercam

Two transits of NGTS-4 were observed with Eulercam on the 1.2 m Euler Telescope at La Silla Observatory. The observations took place on the nights beginning 2018 April 15 and 2018 April 19. Both transits were observed using the same broad NGTS filter that was used to obtain the discovery photometry. For the first observation a total of 193 images were obtained using a 40 s exposure and 0.1 mm defocus. For the second observation a total of 140 images were obtained using a 55 s exposure time and 0.1 mm defocus.

The data were reduced using the standard procedure of bias subtraction and flat-field correction. Aperture photometry was performed with the PyRAF implementation of the phot routine. PyRAF was also used to extract information useful for de-trending; X- and Y-position, FWHM, airmass and sky background of the target star. The comparison stars and the photometric aperture radius were chosen in order to minimise the RMS in the scatter out of transit. Additional checks were made with different comparison star ensembles, aperture radii and with stars in the FOV expected to show no variation. This was to ensure the transit signal was not an artefact of these choices. The resulting light-curves are plotted in Figure 4, showing a detection of a full transit signature in the data from 2018 April 19, though the detection in the data from 2018 April 15 is marginal at best.

4 SPECTROSCOPY

We obtained multi-epoch spectroscopy for NGTS-4 with the HARPS spectrograph (Mayor et al. 2003) on the ESO 3.6 m telescope at La Silla Observatory, Chile, between 2017 December 01 and 2018 April 10 under programme ID 0101.C-0623(A).

We used the standard HARPS data reduction software (DRS) to the measure the radial velocity of NGTS-4 at each epoch. This was done via cross-correlation with the K0 binary mask. The exposure times for each spectrum were 2700 s. The radial velocities are listed, along with their associated error, FWHM, contrast, bisector span and exposure time in Table 3.

The 14 radial velocity measurements show a variation in-phase with the period detected by ORION. With a semi-amplitude of $13.7 \pm 1.9\,\mathrm{m\,s^{-1}}$ they indicate a Neptune-mass transiting planet (see Figure 2). To ensure that the radial velocity signal originates from a planet orbiting NGTS-4 we analysed the HARPS cross correlation functions (CCF) using the line bisector technique of Queloz et al. (2001). We find no evidence for a correlation between the radial velocity and the bisector spans (see Figure 3).

In order to characterise the stellar properties of NGTS-4 we wavelength shift and combine all 14 HARPS spectra to create a high signal-to-noise spectrum for analysis in Section 5.1.

5 ANALYSIS

5.1 Stellar Properties

5.1.1 Spectroscopic stellar parameters

The HARPS spectra were analysed using SPECIES (Soto & Jenkins 2018). This is a python tool to derive stellar parameters in an automated way, from high resolution echelle spectra. SPECIES measures the equivalent widths (EWs) for a list of FeI and FeII lines using ARES (Sousa et al. 2015), and they are input into MOOG (Sneden 1973), along with ATLAS9 model atmospheres (Castelli & Kurucz 2004), to solve the radiative transfer equation. The correct set of atmospheric parameters (T_{eff}, $\log g$, $[Fe/H]$) are reached when no correlations exist between the obtained abundances for each line, the line excitation potential and the reduced EW (EW/λ), and the abundance of neutral and ionized iron agree. Mass and radius are found by interpolating through a grid of MIST isochrones (Dotter 2016), using a Bayesian approach. The atmospheric parameters, along with the extinction corrected magnitudes and the Gaia parallax listed in Table 4, were used as priors. The extinction for each band was computed using the maps from Bovy et al. (2016). Finally, the rotational and macroturbulent velocity were derived using the relation from dos Santos et al. (2016), and by line fitting to a set of five absorption lines. SPECIES gives a stellar radius of $0.84 \pm 0.01\,\mathrm{R_\odot}$ and a metallicity of -0.28 ± 0.10 dex. The stellar parameters measured by SPECIES are listed in Table 4.

5.1.2 Kinematics and Environment

Using the Gaia parallax and the tables of Bailer-Jones et al. (2018) we estimate the distance to NGTS-4 to be 282.6 ± 1.8 parsec.

NGTS-4 has a relatively high proper motion, consistent with what we expect for the estimated distance and spectral type, of $-16.881 \pm 0.034\,\mathrm{mas\,yr^{-1}}$ and $-7.371 \pm 0.036\,\mathrm{mas\,yr^{-1}}$ in R.A. and Dec. respectively. It has a very high systemic radial velocity as determined from our HARPS observations ($111.2 \pm 0.2\,\mathrm{km\,s^{-1}}$) and confirmed from Gaia DR2 ($110.5 \pm 5.5\,\mathrm{km\,s^{-1}}$).

Table 2. A summary of the follow-up photometry of NGTS-4

Night	Site	Instrument	N_{images}	Exptime (seconds)	Binning	Filter	Comment
2017 Nov 27	SAAO	SHOC	360	30	4×4	V	full transit
2018 Apr 15	CTIO	LCO 1m	31	180	1×1	i	mid+egress
2018 Apr 15	Paranal	Speculoos/Callisto	471	12	1×1	I+z	full transit
2018 Apr 15	Paranal	Speculoos/Europa	473	12	1×1	I+z	full transit
2018 Apr 15	La Silla	Eulercam	193	40	1×1	NGTS	full transit
2018 Apr 16	SSO	LCO 1m	19	180	1×1	i	egress
2018 Apr 19	CTIO	LCO 1m	11	180	1×1	i	ingress
2018 Apr 19	La Silla	Eulercam	140	55	1×1	NGTS	full transit
2018 Apr 20	SSO	LCO 1m	16	180	1×1	i	egress
2018 Apr 22	SAAO	SHOC	2160	2	4×4	I	egress
2018 Apr 27	CTIO	LCO 1m	19	180	1×1	i	egress
2018 May 06	SSO	LCO 1m	15	180	1×1	i	egress
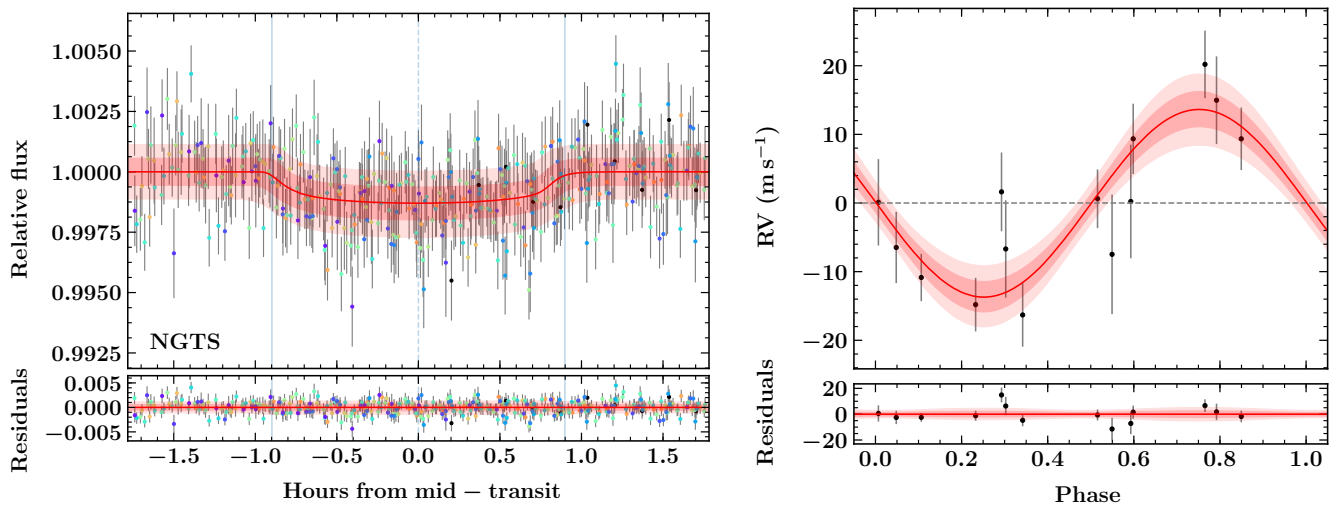
Figure 2. Left: De-trended NGTS discovery photometry with the GP-EBOP model's transit component in red. The data are binned to 10 min cadence, with individual transits colour-coded. Right: HARPS radial velocity data with the best-fit circular orbit model. In both cases, the red lines and pink shaded regions show the median and the 1σ and 2σ confidence intervals of GP-EBOP's posterior model.

Table 3. HARPS Radial Velocities for NGTS-4

| BJD$_{TDB}$ (-2,400,000)	RV (km s^{-1})	RV err (km s^{-1})	FWHM (km s^{-1})	Contrast	BIS (km s^{-1})	Exptime (seconds)
58088.796126	111.20332	0.00428	6.05296	42.601	-0.02945	2700
58090.790319	111.20280	0.00629	6.02478	40.836	-0.00521	2700
58091.804515	111.22290	0.00492	6.05677	41.368	-0.04256	2700
58113.827181	111.18789	0.00390	6.03459	42.909	-0.01615	2700
58125.694569	111.19185	0.00345	6.06011	42.884	-0.01553	2700
58127.682623	111.20292	0.00828	6.02870	42.492	-0.03770	2700
58160.714908	111.20432	0.00574	6.01184	42.535	-0.03220	2700
58162.719953	111.21767	0.00639	6.03778	42.665	-0.03507	2700
58189.543826	111.21205	0.00456	6.03951	43.090	-0.02321	2700
58190.545562	111.21205	0.00512	6.05674	42.993	-0.00393	2700
58199.563729	111.18639	0.00463	6.05506	42.778	-0.05251	2700
58215.559376	111.19600	0.00710	6.04539	43.125	-0.05181	2700
58216.556670	111.19622	0.00519	6.03521	43.087	-0.03327	2700
58218.564257	111.19522	0.00870	6.08229	43.049	0.00362	2700
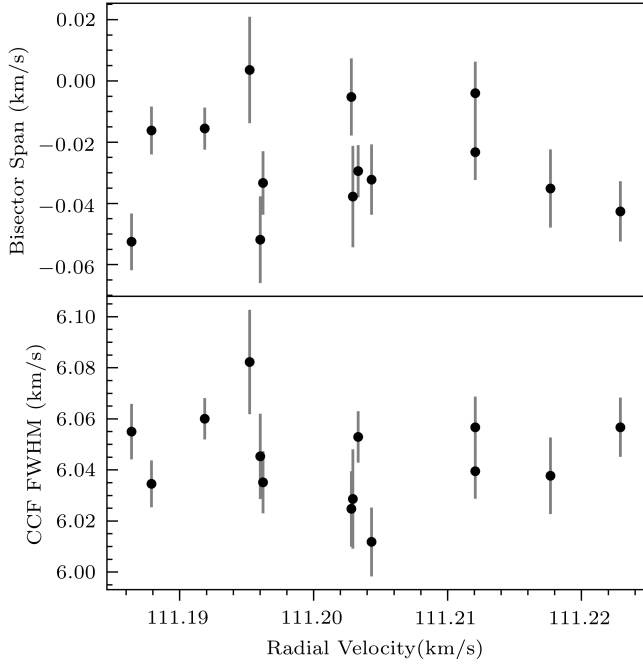
Figure 3. Top: HARPS CCF bisector slopes for the spectra in Table 3, plotted against radial velocity. We find no trend in the bisectors with radial velocity, which can be indicative of a blended system. Bottom: CCF FWHM for the same HARPS spectra. The FWHM of the HARPS CCFs are essentially constant.

When combined with the Gaia DR2 parallax (Gaia Collaboration et al. 2018a), we derived the following Galactic velocity components $(U_{LSR}, V_{LSR}, W_{LSR})$ with respect to the Local Standard of Rest to be $(66.99 \pm 0.10, -72.46 \pm 0.15, -38.22 \pm 0.08)\,\mathrm{km\,s^{-1}}$, assuming the Local Standard of Rest is UVW=(11.1, 12.24, 7.25) $\mathrm{km\,s^{-1}}$ from Schönrich et al. (2010). This suggests that NGTS-4 is a member of the thick disk population (V_{tot} = 105.8 $\mathrm{km\,s^{-1}}$, see e.g. Gaia Collaboration et al. 2018b) similar to NGTS-1 (Bayliss et al. 2018).

There are no other sources within 15″ of NGTS-4 in the Gaia DR2 catalogue. This means we can rule out any blended object down to a Gaia magnitude of approximately G=20.7 beyond 2″ and within the NGTS photometric aperture. However, the Gaia DR2 completeness for close companions falls off within 2″ and is zero within 0.5″ (Arenou et al. 2018).

5.2 Global Modelling

To obtain fundamental parameters for NGTS-4b, we modelled the light and radial velocity curves of NGTS-4 using GP-EBOP (Gillen et al. 2017). These comprise the NGTS discovery light curve, 12 follow-up light curves from six 1m-class telescopes, and 14 HARPS RVs (as set out in Sect. 2, 3 and 4). GP-EBOP comprises a central transiting planet and eclipsing binary model, which is coupled with a Gaussian process (GP) model, and wrapped within an MCMC. Limb darkening (LD) is incorporated using the analytic method of Mandel & Agol (2002) for the quadratic law with the

Table 4. Stellar Properties for NGTS-4

Property	Value	Source
Astrometric Properties		
R.A.	$05^{\mathrm{h}}58^{\mathrm{m}}23\overset{\mathrm{s}}{.}76$	2MASS
Dec	$-30°48'42''\!.49$	2MASS
2MASS I.D.	05582375-3048424	2MASS
Gaia source I.D.	2891248292906892032	Gaia DR2
$\mu_{\mathrm{R.A.}}$ $(\mathrm{mas\,yr^{-1}})$	-16.881 ± 0.034	Gaia DR2
$\mu_{\mathrm{Dec.}}$ $(\mathrm{mas\,yr^{-1}})$	-7.371 ± 0.036	Gaia DR2
γ_{gaia} $(\mathrm{km\,s^{-1}})$	110.5 ± 5.5	Gaia DR2
Parallax (mas)	3.536 ± 0.023	Gaia DR2
Distance (parsec)	282.6 ± 1.8	Gaia DR2
Photometric Properties		
V (mag)	13.14 ± 0.03	APASS
B (mag)	13.95 ± 0.05	APASS
g (mag)	13.48 ± 0.02	APASS
r (mag)	12.91 ± 0.07	APASS
i (mag)	12.64 ± 0.09	APASS
G (mag)	12.91	Gaia DR2
G_{RP} (mag)	12.31	Gaia DR2
G_{BP} (mag)	13.36	Gaia DR2
NGTS (mag)	12.59 ± 0.01	this work
J (mag)	11.58 ± 0.02	2MASS
H (mag)	11.14 ± 0.02	2MASS
K (mag)	11.07 ± 0.02	2MASS
W1 (mag)	11.03 ± 0.02	WISE
W2 (mag)	11.09 ± 0.02	WISE
W3 (mag)	10.98 ± 0.11	WISE
Derived Properties		
T_{eff} (K)	5143 ± 100	SPECIES
$[M/H]$	-0.28 ± 0.10	SPECIES
$v \sin i$ $(\mathrm{km\,s^{-1}})$	2.75 ± 0.58	SPECIES
γ_{RV} $(\mathrm{km\,s^{-1}})$	111.2 ± 0.2	Global modelling
$\log g$	4.5 ± 0.1	SPECIES
$M_*(\mathrm{M_\odot})$	0.75 ± 0.02	SPECIES
$R_*(\mathrm{R_\odot})$	0.84 ± 0.01	SPECIES
ρ_* $(\mathrm{g\,cm^{-3}})$	1.79 ± 0.14	SPECIES
v_{mac}	1.40 ± 0.58	SPECIES
Distance (pc)	282.6 ± 1.8	Gaia DR2

2MASS (Skrutskie et al. 2006); WISE (Wright et al. 2010);
APASS (Henden & Munari 2014);
Gaia DR2 (Gaia Collaboration et al. 2018a)
and Mann et al. (2015)

profiles and uncertainties constrained by the predictions of LDtk (Parviainen & Aigrain 2015).

Most stars are intrinsically variable, which can affect the apparent shape and depth of planet transits. The more active the star, or the higher the level of instrumental systematics, or the shallower the transit signal, the greater the effect on the transit modelling and hence the inferred planet parameters. NGTS-4 is a relatively quiet star and the NGTS systematics are low, but the transit signal is very shallow. Furthermore, the 12 follow-up light curves obtained from 6 facilities all have their own level of systematics and hence correlated noise. GP-EBOP is designed to propagate the effect of variability/systematics into the inferred stellar and planet properties. The reader is referred to Gillen et al. (2017) for further details on the model.

We modelled the orbit of NGTS-4b assuming both a circular and an eccentric orbit about the host star. Both models were identical except for the orbital eccentricity constraints. Each light curve was given its own variability/systematics

Table 5. Planetary properties for NGTS-4b for a circular orbit and eccentric orbit. We adopt the circular model as the most likely solution, the parameters from the eccentric model are provided for information only.

Property	Value (circular)	Value (ecc)
P (days)	1.3373508 ± 0.000008	1.3373506 ± 0.000008
T_C (HJD)	2457607.9975 ± 0.0034	2457607.9978 ± 0.0033
T_{14} (hours)	1.80 ± 0.10	1.79 ± 0.09
a/R_*	4.79 ± 1.21	4.22 ± 1.18
K (m s^{-1})	13.7 ± 1.9	14.0 ± 2.0
e	0.0 (fixed)	$0.14^{+0.18}_{-0.10}$
ω (deg)	0.0 (fixed)	69^{+35}_{-92}
$M_p (M_\oplus)$	20.6 ± 3.0	20.8 ± 3.4
$R_p (R_\oplus)$	3.18 ± 0.26	3.18 ± 0.27
R_p/R_*	0.035 ± 0.003	0.035 ± 0.003
ρ_p (g cm^{-3})	3.45 ± 0.95	3.50 ± 0.95
ρ_* (g cm^{-3})	1.91 ± 0.16	1.91 ± 0.16
a (AU)	0.019 ± 0.005	0.017 ± 0.004
T_{eq}(K)	1650 ± 400	1650 ± 400
i (deg)	82.5 ± 5.8	81.0 ± 7.7

model (with the exception of the LCO light curves which, given the observational uncertainties, all shared the same GP variability model). A Matern-32 kernel was chosen for all light curves given the low level of apparent stellar variability but clear presence of instrument systematics and/or atmospheric variability. Limb darkening profiles were generated using LDtk, given estimates of T_{eff}, $\log g$ and [Fe/H] from SPECIES (see Sect. 5.1). The LD uncertainty was inflated by a factor of 10 to account for systematic uncertainties in stellar atmosphere models around where NGTS-4 lies. The NGTS light curve was binned to 10 min cadence and all other light curves to 3 min cadence, with the GP-EBOP model integrated accordingly. The 14 HARPS RVs were modelled with a Keplerian orbit where the uncertainties were allowed to inflate, if required. We ran the MCMC for 80 000 steps with 200 walkers, discarding the first 30 000 points as burn in and using a thinning factor of 500.

We find that the derived planet parameters from both the circular and eccentric models are consistent to within their 1σ uncertainties. Furthermore, the eccentric model converges on an eccentricity consistent with zero at the 1.5σ level, which suggests that there is no clear evidence for an eccentric orbit in our data. We therefore adopt the circular model as our main model.

We find that NGTS-4b comprises a $20.6 \pm 3.0 \, M_\oplus$ and $3.18 \pm 0.26 \, R_\oplus$ planet, with a corresponding density of $3.45 \pm 0.95 \, \text{g cm}^{-3}$, which orbits NGTS-4 in $1.3373508 \pm 0.000008 \, \text{d}$ with a semi-major axis of $0.019 \pm 0.005 \, \text{AU}$. Fitted and derived parameters of the GP-EBOP model are reported in Table 5. The best-fit GP-EBOP models are plotted against the de-trended NGTS discovery photometry and the HARPS radial velocity data are presented in Figure 2, and against the de-trended 1 m-class follow-up photometry in Figure 4. The light curve data in these plots has been de-trended with respect to GP-EBOP's variability model and, accordingly, the GP-EBOP model displayed is the posterior transit component alone.

In addition to the circular fit, we also present the results of the eccentric model fit in Table 5. We suspect that the fitted non-zero eccentricity in this model is due to the spar-

sity of RV coverage at an orbital phase of ∼0.9. Nevertheless, given that the orbit of such a short-period planet as NGTS-4b would be expected to have circularised, an eccentric orbit if true would be potentially interesting.

6 DISCUSSION

NGTS-4b is the shallowest transiting exoplanet so far discovered from the ground (see Figure 5), with a transit depth of just 0.13 ± 0.02 %. It is approximately 30% shallower than the second shallowest discovery - KELT-11b (Gaudi et al. 2017). The ability to be able to detect such shallow transits allows NGTS to reach down into the Neptunian desert, as evidenced by NGTS-4b, in a way that has not previously been possible for ground-based surveys. It is also encouraging for prospects of following up shallow *TESS* discoveries using the NGTS facility.

Figure 6 shows the masses and radii of known transiting planets that have masses measured to better than 30%, along with mass-radius relations from the models of Seager et al. (2007). The mass and radius of NGTS-4b as measured in this work are consistent with a composition of 100% H_2O, however this is likely to be unphysical given the proximity to the host star, and it is more likely to consist of a rocky core with a water and/or gaseous envelope.

Studies have reported a significant dearth of Neptune-sized ($R < 5 \, R_\oplus$) planets in close orbits (P< 3 d), the so-called "Neptunian desert" (Mazeh et al. 2016), perhaps due to the X-ray/EUV flux from the host stars quickly stripping these planets of their atmospheres and leaving them as lower-mass rocky cores. However as can been seen from Figure 7, NGTS-4b is clearly in a central region of the Neptunian desert, and is likely to still contain a significant atmosphere despite its proximity to its host star. There is nothing in our photometric or spectroscopic data to suggest that NGTS-4 is particularly young, so it is unlikely that this can explain the existence of NGTS-4b in the Neptunian desert.

Following the method of King et al. (2018), and assuming a canonical evaporation efficiency of 15 per cent and the X-ray-age relations of Jackson et al. (2012), we estimate a mass loss rate of $10^{10} \, \text{g s}^{-1}$, even at an assumed age of 5 Gyr. This is at least an order of magnitude higher than the inferred mass loss rate of the Neptune GJ 436b, which was observed to have a 56% deep transit in Lyman-alpha, corresponding to an extended comet-like tail of evaporating material (Ehrenreich et al. 2015; Lavie et al. 2017).

The X-ray luminosity of the star will have been two orders of magnitude higher during its early evolution, when it was maximally active (e.g. Jackson et al. 2012). NGTS-4b may have survived in the Neptunian desert due to an unusually high core mass (e.g. Owen & Lai 2018), or it might have migrated to its current close-in orbit after this epoch of maximum stellar activity (e.g. Jackson et al. 2012).

Future discoveries from NGTS and *TESS* of more Neptune-sized exoplanets should allow us to more carefully characterise the Neptunian desert and the systems that reside within it. The *TESS* mission (Ricker et al. 2014) is set to deliver a large number of transiting exoplanets, the bulk of which will be much shallower than can be detected from ground-based surveys (see Figure 5). However the discovery of NGTS-4b shows that the NGTS facility is able to
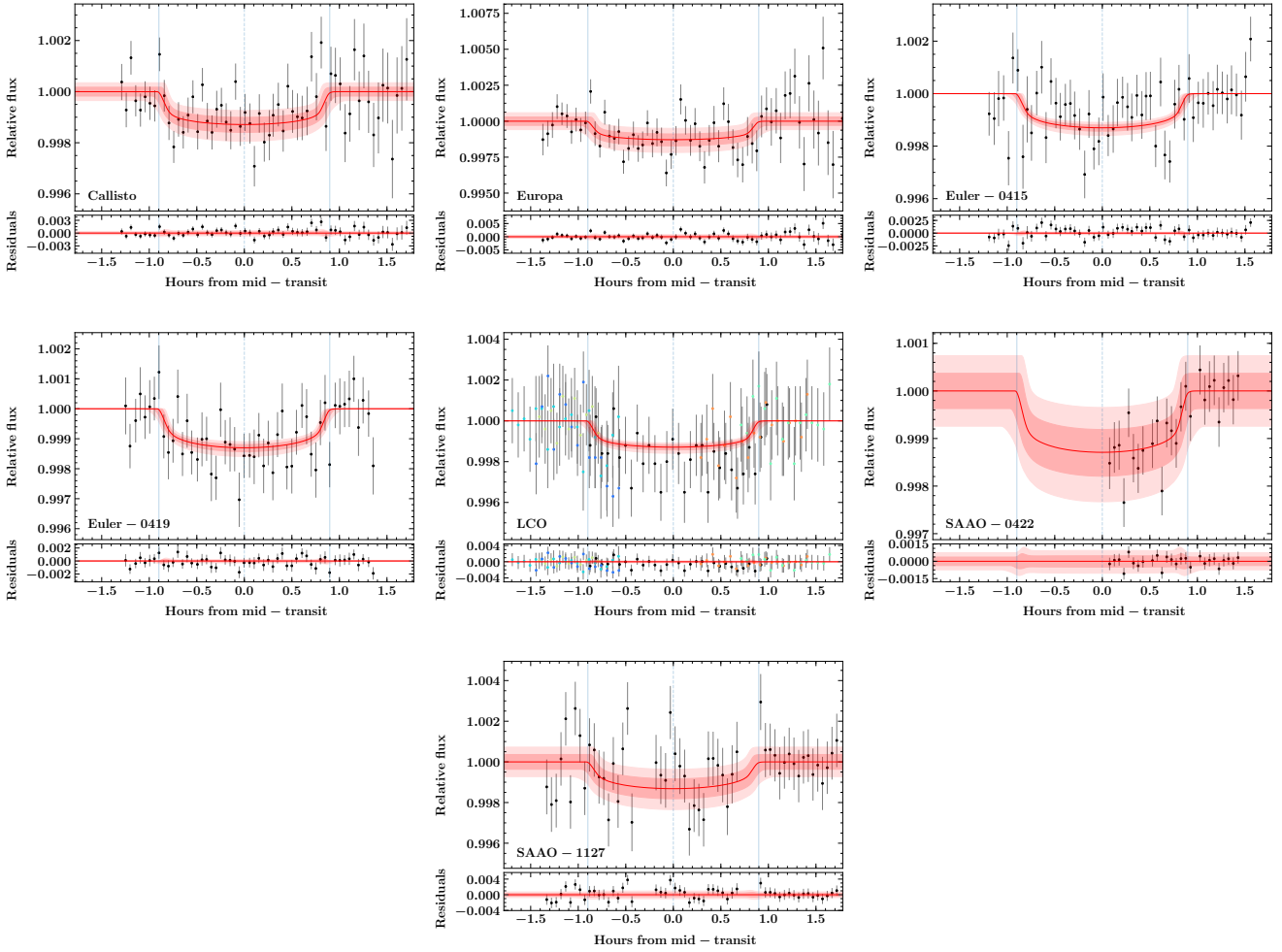
Figure 4. De-trended photometry from the SPECULOOS, EULER, LCO and SAAO follow-up observations, plotted with the GP-EBOP model's transit component. The red lines and pink shaded regions show the median and the 1σ and 2σ confidence intervals of GP-EBOP's posterior model.

detect shallow transits in the magnitude range where many of the *TESS* candidates reside. This will be particularly important for follow-up of single-transit candidates. Villanueva et al. (2018) estimate over 1000 single-transit candidates from *TESS* of which 90% will be deeper than 0.1%. Such candidates will be amenable to follow-up with NGTS.

7   CONCLUSIONS

We have presented the discovery of NGTS-4b, a sub-Neptune-sized transiting exoplanet located within the Neptunian Desert. The discovery of NGTS-4b is a breakthrough for ground-based photometry; the 0.13 ± 0.02 per cent transit being the shallowest ever detected from a wide-field ground-based photometric survey. It allows us to begin to probe the Neptunian desert and find rare exoplanets that reside in this region of parameter space. In the near future, such key systems will allow us to place constraints on planet formation and evolution models and allow us to better understand the observed distribution of planets. Together with future planet detections by NGTS and *TESS* we will

get a much clearer view on where the borders of the Neptunian desert are and how they depend on stellar parameters.

Figure 5. Transit depth versus host star brightness for all transiting exoplanets discovered by wide-field ground-based transit surveys. NGTS-4b is marked in red. Data from NASA Exoplanet Archive (Akeson et al. 2013) accessed on 2018 May 10. The grey dots show the simulated distribution of planet detections from *TESS* (Barclay et al. 2018).
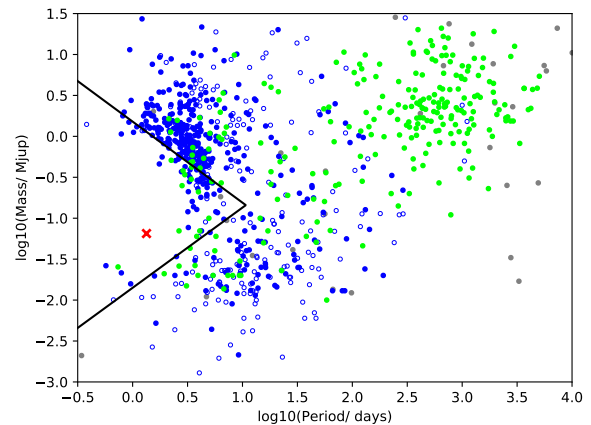

Figure 7. Distribution of mass versus orbital period for planets with a measured mass. Planets discovered by the transit method are shown in blue, with those having masses measured to better than 30% represented as filled circles. Planets found by radial velocity are shown as green circles and those detected by other methods are shown by grey circles. Black lines represent the Neptunian desert as defined in Mazeh et al. (2016). NGTS-4b is shown as a red cross. Taken from the NASA Exoplanet Archive on 2018 August 14.

Figure 6. The mass and radius for all known transiting planets that have fractional errors on the measured planet mass better than 30 %. The black and grey points show discoveries from ground-based and space-based telescopes respectively. The coloured lines show the theoretical mass-radius relation for solid exoplanets of various compositions (Seager et al. 2007). NGTS-4b is highlighted in red.

REFERENCES

Akeson R. L., et al., 2013, PASP, 125, 989

Arenou F., et al., 2018, preprint, (`arXiv:1804.09375`)

Bailer-Jones C. A. L., Rybizki J., Fouesneau M., Mantelet G., Andrae R., 2018, AJ, 156, 58

Bakos G., Noyes R. W., Kovács G., Stanek K. Z., Sasselov D. D., Domsa I., 2004, PASP, 116, 266

Bakos G. Á., et al., 2010, ApJ, 710, 1724

Bakos G. Á., et al., 2013, PASP, 125, 154

Barbary K., 2016, SEP: Source Extractor as a library, The Journal of Open Source Software, doi:10.21105/joss.00058

Barclay T., Pepper J., Quintana E. V., 2018, preprint, (`arXiv:1804.05050`)

Bayliss D., et al., 2018, MNRAS, 475, 4467

Bertin E., Arnouts S., 1996, A&AS, 117, 393

Bovy J., Rix H.-W., Green G. M., Schlafly E. F., Finkbeiner D. P., 2016, ApJ, 818, 130

Brown T. M., et al., 2013, PASP, 125, 1031

Burdanov A., Delrez L., Gillon M., Jehin E., Speculoos T., Trappist Teams 2017, SPECULOOS Exoplanet Search and Its Prototype on TRAPPIST. p. 130, doi:10.1007/978-3-319-30648-3_130-1

Castelli F., Kurucz R. L., 2004, ArXiv Astrophysics e-prints,

Chazelas B., et al., 2012, in Ground-based and Airborne Telescopes IV. p. 84440E, doi:10.1117/12.925755

Collier Cameron A., et al., 2006, MNRAS, 373, 799

Coppejans R., et al., 2013, Publications of the Astronomical Society of the Pacific, 125, 976

Craig M. W., et al., 2015, ccdproc: CCD data reduction software, Astrophysics Source Code Library (ascl:1510.007)

Delrez L., et al., 2018, in Society of Photo-Optical Instrumentation Engineers (SPIE) Conference Series. p. 107001I (`arXiv:1806.11205`), doi:10.1117/12.2312475

Dotter A., 2016, ApJS, 222, 8

Ehrenreich D., et al., 2015, Nature, 522, 459

Fulton B. J., Petigura E. A., 2018, preprint, p. arXiv:1805.01453 (`arXiv:1805.01453`)

Gaia Collaboration et al., 2018b, preprint, (`arXiv:1804.09378`)

Gaia Collaboration Brown A. G. A., Vallenari A., Prusti T., de Bruijne J. H. J., Babusiaux C., Bailer-Jones C. A. L., 2018a, preprint, (`arXiv:1804.09365`)

Gaudi B. S., et al., 2017, Nature, 546, 514

Gillen E., Hillenbrand L. A., David T. J., Aigrain S., Rebull L., Stauffer J., Cody A. M., Queloz D., 2017, ApJ, 849, 11

Gillon M., et al., 2013, A&A, 552, A82

Gillon M., et al., 2016, Nature, 533, 221

Grether D., Lineweaver C. H., 2006, ApJ, 640, 1051

Günther M. N., et al., 2017, MNRAS, 472, 295

Henden A., Munari U., 2014, Contributions of the Astronomical Observatory Skalnate Pleso, 43, 518

Irwin J., Charbonneau D., Nutzman P., Falco E., 2009, in Pont F., Sasselov D., Holman M. J., eds, IAU Symposium Vol. 253, Transiting Planets. pp 37–43 (`arXiv:0807.1316`), doi:10.1017/S1743921308026215

Jackson A. P., Davis T. A., Wheatley P. J., 2012, MNRAS, 422, 2024

King G. W., et al., 2018, MNRAS, 478, 1193

Kovács G., Zucker S., Mazeh T., 2002, A&A, 391, 369

Kurokawa H., Nakamoto T., 2014, ApJ, 783, 54

Lavie B., et al., 2017, A&A, 605, L7

Lecavelier Des Etangs A., 2007, A&A, 461, 1185

Lopez E. D., Fortney J. J., 2014, ApJ, 792, 1

Mandel K., Agol E., 2002, ApJ, 580, L171

Mann A. W., Feiden G. A., Gaidos E., Boyajian T., von Braun K., 2015, ApJ, 804, 64

Mayor M., et al., 2003, The Messenger, 114, 20

Mazeh T., Holczer T., Faigler S., 2016, A&A, 589, A75

McCormac J., Pollacco D., Skillen I., Faedi F., Todd I., Watson C. A., 2013, arXiv

McCormac J., et al., 2017, PASP, 129, 025002

Nutzman P., Charbonneau D., 2008, PASP, 120, 317

Owen J. E., Lai D., 2018, MNRAS, p. 1685

Parviainen H., Aigrain S., 2015, MNRAS, 453, 3821

Pepper J., et al., 2007, PASP, 119, 923

Pepper J., Kuhn R. B., Siverd R., James D., Stassun K., 2012, PASP, 124, 230

Pollacco D. L., et al., 2006, PASP, 118, 1407

Queloz D., et al., 2001, A&A, 379, 279

Ricker G. R., et al., 2014, in Space Telescopes and Instrumentation 2014: Optical, Infrared, and Millimeter Wave. p. 914320 (`arXiv:1406.0151`), doi:10.1117/12.2063489

Schönrich R., Binney J., Dehnen W., 2010, MNRAS, 403, 1829

Seager S., Kuchner M., Hier-Majumder C. A., Militzer B., 2007, ApJ, 669, 1279

Skrutskie M. F., et al., 2006, AJ, 131, 1163

Sneden C. A., 1973, PhD thesis, THE UNIVERSITY OF TEXAS AT AUSTIN.

Soto M. G., Jenkins J. S., 2018, preprint, (`arXiv:1801.09698`)

Sousa S. G., Santos N. C., Adibekyan V., Delgado-Mena E., Israelian G., 2015, A&A, 577, A67

Stetson P. B., 1987, PASP, 99, 191

Szabó G. M., Kiss L. L., 2011, ApJ, 727, L44

Tamuz O., Mazeh T., Zucker S., 2005, MNRAS, 356, 1466

Villanueva Jr. S., Dragomir D., Gaudi B. S., 2018, preprint, (`arXiv:1805.00956`)

Wheatley P. J., et al., 2013, in European Physical Journal Web of Conferences. p. 13002 (`arXiv:1302.6592`), doi:10.1051/epjconf/20134713002

Wheatley P. J., et al., 2018, MNRAS, 475, 4476

Wright E. L., et al., 2010, AJ, 140, 1868

dos Santos L. A., et al., 2016, A&A, 592, A156

This paper has been typeset from a TEX/LATEX file prepared by the author.